

Global Symmetry and Orthogonal Transformations from Geometrical Moment n -tuples

Omar Tahri^a

^aICB UMR CNRS 6303, Université de Bourgogne, 9 Av. Alain Savary, Dijon, 21000, Bourgogne, France

Abstract

Detecting symmetry is crucial for effective object grasping for several reasons. Recognizing symmetrical features or axes within an object helps in developing efficient grasp strategies, as grasping along these axes typically results in a more stable and balanced grip, thereby facilitating successful manipulation. This paper employs geometrical moments to identify symmetries and estimate orthogonal transformations, including rotations and mirror transformations, for objects centered at the frame origin. It provides distinctive metrics for detecting symmetries and estimating orthogonal transformations, encompassing rotations, reflections, and their combinations. A comprehensive methodology is developed to obtain these functions in n -dimensional space, specifically moment n -tuples. Extensive validation tests are conducted on both 2D and 3D objects to ensure the robustness and reliability of the proposed approach. The proposed method is also compared to state-of-the-art work using iterative optimization for detecting multiple planes of symmetry. The results indicate that combining our method with the iterative one yields satisfactory outcomes in terms of the number of symmetry planes detected and computation time.

Keywords:

Symmetry detection, orthogonal transformations, geometrical moments, n -dimensional space

1. Introduction

The problem of extracting geometrical features holds a prominent position within the literature of pattern recognition. Specifically, the identification of characteristics such as symmetry or orthogonal transformations remains pertinent across various domains. For instance, symmetrical properties find utility in fields such as chemistry, where they are leveraged in the design of expansive protein domains Fortenberry et al. (2011). Additionally, in structural engineering, the discovery of symmetries within polygonal structures serves as a significant aspect Zhang et al. (2022). These symmetries are also integral to structure-aware processing, as highlighted by Mitra et al. (2014), as they constitute a fundamental source for generating structural patterns. Moreover, within the computational domain, symmetry detection emerges as a critical feature, notably in constraint programming Gent et al. (2006) and linear programming. Such detection aids in problem simplification, as emphasized by Margot (2009).

Email address: otahri@gmail.com (Omar Tahri)

In general, the search for a robust model capable of detecting symmetry holds significance across various domains such as computer graphics, computer vision, machine learning Liu et al. (2010), and robotics. For instance, in the domain of object pose estimation, symmetry properties have been effectively utilized to identify matching correspondences, as demonstrated by Song et al. (2020). Additionally, Huang et al. (2014) proposed a method leveraging symmetries for automatic image completion, highlighting the broad applicability of symmetry detection techniques. Furthermore, applications including object completion Speciale et al. (2016) and model compression Tayangkanon et al. (2018); Wang et al. (2015a) also stand to benefit from the exploitation of symmetries and orthogonal transformations.

Robotics field also exploits these features for extracting object properties. This is fundamental to predict their behavior when they are in motion. For instance, detecting objects symmetries will contribute developing better grasping and manipulation strategies Lederman and Wing (2003); Li et al. (2005).

The literature encompasses a multitude of specialized methodologies owing to the extensive range of applications. For instance, certain researchers, such as those in Atallah (1985); Wolter et al. (1985), focus on estimating perfect symmetry, while others, as Alt et al. (1988), address the estimation of approximate global symmetry within discrete sets of points. Addressing the 2D scenario, Derrode and Ghorbel (2004) employ the Fourier-Mellin transform to assess motion parameters encompassing rigid transformations and reflection symmetries. Alternatively, some researchers opt for feature matching techniques to estimate rotational and reflection symmetries in 2D images, as demonstrated in Shen et al. (1999) employing features derived from the first three nonzero generalized complex (GC) moments. Additionally, the Slope Chain approach has garnered attention in the literature Aguilar et al. (2020), although its efficacy is compromised when dealing with quasi-symmetrical distributions. Proposing a distinct methodology, Wang et al. (2015b) present a method for detecting reflection symmetry via the correspondence of locally affine invariant edge-based features. In another vein, Widynski et al. (2014) advocate for utilizing contours of ribbon-like 2D objects within 2D images to discern smooth local symmetries. Furthermore, recent advancements have seen the emergence of neural network-based approaches for symmetry detection, as exemplified by the work of Krippendorf and Syvaeri (2020).

In three-dimensional (3D) space, Ecins et al. (2017) propose employing symmetrical fitting as a methodology for designing a reflection symmetry detection technique. Additionally, methods have been introduced for detecting global reflection in 3D point clouds Nagar and Raman (2020a). Ji and Liu (2019) advocate for a neural network-based approach aimed at detecting 3D reflection symmetry planes through pointwise classification. Continuing along this idea, Zhou et al. (2021) propose a neural network architecture utilizing ResNet as its backbone. Conversely, Gao et al. (2020) leverage a convolutional neural network (CNN), with emphasis placed on refining the loss function. Other approaches, such as that proposed by Shi et al. (2020), rely on numerical optimization techniques, leveraging symmetry priors to address reconstruction challenges in noisy input scenarios. Alternatively, closed-form methodologies are also evident in the literature, exploiting various geometrical features. For instance, 3D moments have been utilized to deduce symmetry parameters, as evidenced by Martinet et al. (2006). Over the span of more than half a century, theoretical frameworks and applications leveraging moments have thrived across diverse domains, encompassing tasks such as pose estimation Cyganski and Orr (1985); Mukundan and Ramakrishnan (1998), character recognition Wong et al. (1995), target recognition Liu et al. (2012), quality inspection Sluzek (1995), image matching Chen and Sun (2010), multi-sensor fusion Markandey and deFigueiredo (1992), and visual servoing Tahri and Chaumette (2005); Tahri et al. (2010).

The literature also features works that tackle the challenge of symmetry detection in high-dimensional spaces by projecting the problem onto lower-dimensional spaces. Examples include studies such as Zhang et al. (2022); Chen et al. (2017); Zingoni (2012), which identify symmetries within intricate 3D topologies by projecting them onto 2D images. In contrast, our research introduces a comprehensive approach to detecting symmetrical and orthogonal transformations (encompassing rotation and mirror transformations) without the need for mapping input data to lower-dimensional spaces. We present a closed-form solution based on moments that can be applied across various domains regardless of their space dimensionality. Furthermore, as an analytical solution, our approach does not require prior data for model training.

Subsequent to this introduction, we will provide an overview of the framework and its adaptation to each specific problem. Subsequently, to assess the n -dimensional condition, we will conduct a comprehensive analysis across multiple levels, encompassing both 2D and 3D perspectives. Furthermore, the evaluation will be conducted with respect to symmetry patterns, including reflection planes, axes of rotation, or centers of gravity.

2. Geometrical representation using moments

Let define first the fundamentals of the geometrical features used here and how they variate with respect to the motion. Concretely, this work considers the manifold of p -th order moments of an original n -dimensional space.

2.1. Geometrical p -th order moments

Consider, a defined region $\mathbf{X} \subset \mathbb{R}^n$ by a piecewise-continuous real density distribution function $f(\mathbf{X})$ of nonzero values only in a finite region of the original n -dimensional space. Its moments of order $p = \sum_{i=1}^n p_i$ is defined by,

$$m_{p_1 \dots p_n} = \int_{\mathbb{R}^n} \prod_{i=1}^n x_i^{p_i} f(\mathbf{X}) d\mathbf{X}, \quad (1)$$

where $[x_1 \dots x_n]^\top$ are the components of an infinitesimal point $\mathbf{x} \in \mathbf{X}$. The central moments of order p are defined by,

$$\mu_{p_1 \dots p_n} = \int_{\mathbb{R}^n} \prod_{i=1}^n (x_i - \bar{x}_i)^{p_i} f(\mathbf{X}) d\mathbf{X},$$

where each \bar{x}_i is a component of the object gravity center $\bar{\mathbf{x}} = \left[\frac{m_{1,0,\dots,0}}{m_{0,\dots,0}} \quad \frac{m_{0,1,0,\dots,0}}{m_{0,\dots,0}} \quad \dots \quad \frac{m_{0,\dots,1}}{m_{0,\dots,0}} \right]^\top$. Moving the spatial reference frame to this point allows computing centered moments. In the case when the generative function $f(\mathbf{X})$ defines a discrete distribution function, their moments are defined by,

$$m_{p_1 \dots p_n} = \sum_{i=1}^{|\mathbf{X}|} \prod_{j=1}^n x_i^{p_j} f(\mathbf{x}_i) \quad (2)$$

where \mathbf{x}_i is a point of the point set \mathbf{X} and $|\cdot|$ gets the amount of points. The proposed framework in this paper is valid for both continuous and discrete objects, namely a discrete 3D points cloud.

2.2. Orthogonal transformation and rotational speed

The motion of a distribution \mathbf{X} under n -dimensional orthogonal transformation $\mathbf{R} \in \text{SO}(n)$ is expressed as follows,

$$\mathbf{X}' = \mathbf{R}\mathbf{X}. \quad (3)$$

satisfying $\mathbf{R}\mathbf{R}^\top = \mathbb{I}$ and $\det(\mathbf{R}) = 1$. If a rotational speed is applied, then the speed of each point $\dot{\mathbf{X}}$ is given by,

$$\dot{\mathbf{X}} = \mathbf{L}\mathbf{X} \quad (4)$$

where \mathbf{L} is an antisymmetric matrix defined from rotational velocities. Particularly, we have $\dot{\mathbf{x}} = \mathbf{L}_3\mathbf{x} = -[\mathbf{x}]_\times \boldsymbol{\omega}$ and a defined matrix \mathbf{L}_3 using the vector of values $\boldsymbol{\omega} = [\omega_1 \ \omega_2 \ \omega_3]^\top$ of rotation speeds in 3D distributions $\mathbf{X} \subset \mathbb{R}^3$ for the x_2x_3 , x_3x_1 and x_1x_2 planes. Concretely, the antisymmetric defined matrix is defined as follows,

$$\mathbf{L}_3 = \begin{bmatrix} 0 & -\omega_3 & \omega_2 \\ \omega_3 & 0 & -\omega_1 \\ -\omega_2 & \omega_1 & 0 \end{bmatrix} \quad (5)$$

we derive that both eq. 11 and eq. 3 are linearly dependent with respect to the same orthogonal transformation \mathbf{R} .

2.3. Moment time variation and rotational speeds

Considering that an orthogonal transformation in \mathbf{X} , eq. (3), implies motion in its moments. The motion, or time variation, of a moment $\dot{m}_{p_1 \dots p_n}$ Tahri (2004); Tahri and Chaumette (2003) is obtained by differentiating eq. (1),

$$\begin{aligned} \dot{m}_{p_1 \dots p_n} = & \sum_{i=1}^n \int_{\mathbb{R}^n} p_i \dot{x}_i x_i^{p_i-1} \prod_{j=1, j \neq i}^n x_j^{p_j} f(\mathbf{X}) d\mathbf{X} \\ & + \int_{\mathbb{R}^n} \prod_{j=1}^n x_j^{p_j} \dot{f}(\mathbf{X}) d\mathbf{X} + \int_{\mathbb{R}^n} \prod_{j=1}^n x_j^{p_j} f(\mathbf{X}) \left(\sum_{i=1}^n \frac{\partial \dot{x}_i}{\partial x_i} \right) d\mathbf{X} \end{aligned} \quad (6)$$

Because the matrix \mathbf{L} is antisymmetric (the diagonal entries are null), $\frac{\partial \dot{x}_i}{\partial x_i} = 0$, the third term of eq. (6) vanishes when the distribution is subjected to rotational speeds. If we assume that the time derivative of the density function $\dot{f}(\mathbf{x}) = 0$, i.e. the density function in an infinitesimal point does not change under rotation motions, the second term vanishes as well. According to eq. (4), we have $\dot{x}_i = \sum_{j=1}^n l_{ij} x_j$, where l_{ij} are the entries of the matrix \mathbf{L} and combining with eq. (6), the time variation of moment caused by rotational speeds is obtained as,

$$\begin{aligned} \dot{m}_{p_1 \dots p_n} = & \sum_{i=1}^n \sum_{j=1}^n p_i l_{ij} \int_{\mathbb{R}^n} x_i^{p_i-1} x_j \prod_{k=1, k \neq i}^n x_k^{p_k} f(\mathbf{X}) d\mathbf{X} \\ = & \sum_{i=1}^n \sum_{j=1}^n p_i l_{ij} m_{p_1, \dots, p_i-1, \dots, p_j+1, \dots, p_n}. \end{aligned} \quad (7)$$

Using eq. (7) and eq. (5) leads in 3D space to,

$$\begin{aligned} \dot{m}_{p_1 p_2 p_3} = & (p_3 m_{p_1, p_2+1, p_3-1} - p_2 m_{p_1, p_2-1, p_3+1}) \omega_1 \\ & + (p_1 m_{p_1-1, p_2, p_3+1} - p_3 m_{p_1+1, p_2, p_3-1}) \omega_2 \\ & + (p_2 m_{p_1+1, p_2-1, p_3} - p_1 m_{p_1-1, p_2+1, p_3}) \omega_3 \end{aligned}, \quad (8)$$

the time variational moment $\dot{m}_{p_1 p_2 p_3}$.

3. N -tuple descriptors definition

Let assume the existence of a manifold with equivariance orthogonal transformation properties with respect to \mathbf{X} . The elements \mathbf{x}_v of this manifold, called n -tuples, will be described as the linear combinations between a moments vector $\mathbf{v}_{(pp'...)}^{(kk'...)}$ and a set of parameters vectors α_i , such as $\mathbf{x}_v = [\alpha_1 \mathbf{v}_{(pp'...)}^{(kk'...)} \quad \alpha_2 \mathbf{v}_{(pp'...)}^{(kk'...)} \quad \dots \quad \alpha_n \mathbf{v}_{(pp'...)}^{(kk'...)}]^\top$.

If \mathbf{v}_p^1 is the vector composed by all moments $m_{p_1 \dots p_n}$ of order p (described in section 2), that is, only monomials (from the linear combination between different moments) of degree 1. \mathbf{v}_p^2 is defined as the vector composed of the monomials of degree 2 resulting of the combination $\mathbf{v}_p^1 \cdot \mathbf{v}_p^1$. Follows straight-forward to the k -times combination of \mathbf{v}_p^1 which obtains a vector \mathbf{v}_p^k with monomials of degree k . This can be extended to the resulting vector $\mathbf{v}_{(pp')}^{(kk')}$ by the combination of two different order-degree moments vectors \mathbf{v}_p^k and $\mathbf{v}_{p'}^{k'}$. Which generalizes to $\mathbf{v}_{(pp'...)}^{(kk'...)}$ for the combination of multiples moments vectors.

Because we assume equivariance orthogonal transformation condition, we can do a similar reasoning on the orthogonality condition of n -tuples using rotational speed. Equivalent to eq. (4), the motion of a n -tuple \mathbf{x}_v is formulated as,

$$\dot{\mathbf{x}}_v = \mathbf{L}\mathbf{x}_v. \quad (9)$$

Solving eq. (9) and assuming constant speed, i.e. constant matrix \mathbf{L} , we have the following relation,

$$\mathbf{x}_v(t) = \exp(\mathbf{L}_t) \mathbf{x}_v(0), \quad (10)$$

where $\exp(\mathbf{L}_t)$ is the matrix exponentiation of \mathbf{L}_t , $\mathbf{x}_v(0)$ and $\mathbf{x}_v(t)$ are respectively the initial and t value of the n -tuple. Knowing that $\exp(\mathbf{L}_t) = \mathbf{R}$, eq. (10) can be rewritten as,

$$\mathbf{x}_v(t) = \mathbf{R}\mathbf{x}_v(0). \quad (11)$$

4. Orthogonal transformation estimation using n -tuples

Using the above properties Details of the section, say that for the lack of space we will focuss on 3D case, Because the lack of space we will focus the derivation on 3D space n -tuples, called triplet. Thus, triples are formally described as $\mathbf{x}_v = [\alpha_1^\top \mathbf{v} \quad \alpha_2^\top \mathbf{v} \quad \alpha_3^\top \mathbf{v}]^\top \in \mathbb{R}^3$.

4.1. Orthogonal transformations and n -tuples

Let us consider the case of 3D distributions, defined by $\mathbf{X} \subset \mathbb{R}^3$. The central moments of a distribution eq. (2) after rotational motion, eq. (3), can be expressed as a linear combination between a set of original moments and a random orthogonal transformation, eq. (11). For example, taken the simplest triplet $\mathbf{x}_v = [m_{100} \quad m_{010} \quad m_{001}]^\top$ where $\mathbf{v} = \mathbf{v}_{(1)}^{(1)}$, we can write that,

$$\begin{bmatrix} m'_{100} \\ m'_{010} \\ m'_{001} \end{bmatrix} = \begin{bmatrix} r_{11}m_{100} + r_{12}m_{010} + r_{13}m_{001} \\ r_{21}m_{100} + r_{22}m_{010} + r_{23}m_{001} \\ r_{31}m_{100} + r_{32}m_{010} + r_{33}m_{001} \end{bmatrix} = \mathbf{R}\mathbf{x}_v, \quad (12)$$

where r_{ij} refers to the element of column j and row i of the matrix \mathbf{R} . Unfortunately, eq. (12) is null for all possible \mathbf{R} since central moments of order $p = 1$ are null. To overcome this problem, the chosen moments of \mathbf{x}_v must be of order $p > 1$. As discussed above, it is possible to

define different triplets from moments of higher order. For example, a consistent triplet with our hypothesis is $\mathbf{x}_v = [m_{300} + m_{120} + m_{102} \quad m_{210} + m_{030} + m_{012} \quad m_{201} + m_{021} + m_{003}]^\top$ which uses $\mathbf{v} = \mathbf{v}_{(3)}^{(1)}$. According to eq. (1), the first term of \mathbf{x}_v is defined as,

$$m_{300} + m_{120} + m_{102} = \int_{-\infty}^{\infty} \int_{-\infty}^{\infty} \int_{-\infty}^{\infty} x_1 (x_1^2 + x_2^2 + x_3^2) d\mathbf{X}. \quad (13)$$

From eq. (13) arise the relation between the first component of \mathbf{X} , i.e. x_1 , and the first component of its triplet \mathbf{x}_v , i.e. $m_{300} + m_{120} + m_{102}$. Applying eq. (13) to eq. (12) we obtain that,

$$\begin{aligned} m'_{300} + m'_{120} + m'_{102} &= \int_{-\infty}^{\infty} \int_{-\infty}^{\infty} \int_{-\infty}^{\infty} x'_1 (x'_1^2 + x'_2^2 + x'_3^2) d\mathbf{X} \\ &= \int_{-\infty}^{\infty} \int_{-\infty}^{\infty} \int_{-\infty}^{\infty} (r_{11}x_1 + r_{12}x_2 + r_{13}x_3) (x_1^2 + x_2^2 + x_3^2) d\mathbf{X} \\ &= r_{11}(m_{300} + m_{120} + m_{102}) + r_{12}(m_{210} + m_{030} + m_{012}) \\ &\quad + r_{13}(m_{201} + m_{021} + m_{003}) \end{aligned} \quad (14)$$

for the first component. The same approach is applied to the successive components of \mathbf{x}_v as,

$$\begin{cases} m'_{210} + m'_{030} + m'_{012} = r_{21}(m_{300} + m_{120} + m_{102}) \\ \quad + r_{22}(m_{210} + m_{030} + m_{012}) + r_{23}(m_{201} + m_{021} + m_{003}) \\ m'_{201} + m'_{021} + m'_{003} = r_{31}(m_{300} + m_{120} + m_{102}) \\ \quad + r_{32}(m_{210} + m_{030} + m_{012}) + r_{33}(m_{201} + m_{021} + m_{003}) \end{cases} \quad (15)$$

leading us to the proof of equivariance condition for the rest of components. Now, let us in the next following provide a general scheme for defining the n-tuples.

4.2. N-tuple derivation: 3D space case

Defined above the moment time variation, let us consider the following vectors of moments,

$$\begin{aligned} \mathbf{v}_2^1 &= [m_{200} \quad m_{110} \quad \cdots \quad m_{002}]^\top \\ \mathbf{v}_3^1 &= [m_{300} \quad m_{210} \quad m_{201} \quad \cdots \quad m_{003}]^\top \\ \mathbf{v}_{(2,3)}^{(1,1)} &= [m_{300}m_{200} \quad m_{300}m_{110} \quad \cdots \quad m_{003}m_{002}]^\top \end{aligned}$$

where $\mathbf{v}_2^1 \in \mathbb{R}^6$ is composed by the 6 moments of order 2, $\mathbf{v}_3^1 \in \mathbb{R}^{10}$ is composed by the 10 moments of order 3 and $\mathbf{v}_{(2,3)}^{(1,1)} \in \mathbb{R}^{60}$ is composed by the 60 monomials products between the entries of \mathbf{v}_2^1 and \mathbf{v}_3^1 . By examining the monomial component $m_{030}m_{200}$ of vector $\mathbf{v}_{(2,3)}^{(1,1)}$ using eq. (8), we have that,

$$\begin{aligned} \frac{d(m_{030}m_{200})}{dt} &= m_{200}\dot{m}_{030} + m_{030}\dot{m}_{200} = -3m_{200}m_{021}\omega_1 \\ &\quad + 2m_{101}m_{030}\omega_2 + (3m_{120}m_{200} - 2m_{110}m_{030})\omega_3. \end{aligned} \quad (16)$$

Note that the coefficients of ω_i are linear combinations between moments of orders 2 and 3. This keeps true for the time derivative of all entries of $\mathbf{v} = \mathbf{v}_{(2,3)}^{(1,1)}$. What allows us to express in a general form the time derivative of \mathbf{v} , as,

$$\dot{\mathbf{v}} = (\mathbf{L}_v^{\omega_1} \mathbf{v})\omega_1 + (\mathbf{L}_v^{\omega_2} \mathbf{v})\omega_2 + (\mathbf{L}_v^{\omega_3} \mathbf{v})\omega_3, \quad (17)$$

where $\mathbf{L}_v^{\omega_1}$, $\mathbf{L}_v^{\omega_2}$ and $\mathbf{L}_v^{\omega_3}$ are matrices in $\mathbb{R}^{n \times n}$ space, where n is the number of monomials in the vector $\mathbf{v} \in \mathbb{R}^n$, e.g. $\mathbf{L}_v^{\omega_1} \in \mathbb{R}^{60 \times 60}$ for the case of $\mathbf{v} = \mathbf{v}_{(2,3)}^{(1,1)}$. These matrices represent the

1. Define the moment vector $\mathbf{v} = \mathbf{v}_{(pp'p''...)}^{(kk'k''...)}$ such that its degree $p \cdot k + p' \cdot k' + \dots$ is an odd integer since even degrees resolve as null.
2. Compute $\mathbf{L}_v^{\omega_1}$, $\mathbf{L}_v^{\omega_2}$ and $\mathbf{L}_v^{\omega_3}$ using eq. (8),.
3. Solve eq. (19) to obtain the vectors α_1 , α_2 and α_3 , which determine the number of n -tuples.

Table 1: Summarized procedure used to derive n -tuples.

interaction between time variational rotational motion $[\omega_1 \ \omega_2 \ \omega_3]$ and the entries of \mathbf{v} , as was the case for $m_{030}m_{200}$. Therefore, the time variation of $\mathbf{x}_v = [\alpha_1^\top \mathbf{v} \ \alpha_2^\top \mathbf{v} \ \alpha_3^\top \mathbf{v}]^\top$ is given by,

$$\dot{\mathbf{x}}_v = \begin{bmatrix} \alpha_1^\top \mathbf{L}_v^{\omega_1} \mathbf{v} & \alpha_1^\top \mathbf{L}_v^{\omega_2} \mathbf{v} & \alpha_1^\top \mathbf{L}_v^{\omega_3} \mathbf{v} \\ \alpha_2^\top \mathbf{L}_v^{\omega_1} \mathbf{v} & \alpha_2^\top \mathbf{L}_v^{\omega_2} \mathbf{v} & \alpha_2^\top \mathbf{L}_v^{\omega_3} \mathbf{v} \\ \alpha_3^\top \mathbf{L}_v^{\omega_1} \mathbf{v} & \alpha_3^\top \mathbf{L}_v^{\omega_2} \mathbf{v} & \alpha_3^\top \mathbf{L}_v^{\omega_3} \mathbf{v} \end{bmatrix} \begin{bmatrix} \omega_1 \\ \omega_2 \\ \omega_3 \end{bmatrix} \quad (18)$$

Then, we have 9 conditions if eq. (18) is of the same form as eq. (5):

$$\begin{array}{lll} 1) \alpha_1^\top \mathbf{L}_v^{\omega_1} \mathbf{v} = 0 & 2) \alpha_2^\top \mathbf{L}_v^{\omega_1} \mathbf{v} = \alpha_3^\top \mathbf{v} & 3) \alpha_3^\top \mathbf{L}_v^{\omega_1} \mathbf{v} = -\alpha_2^\top \mathbf{v} \\ 4) \alpha_1^\top \mathbf{L}_v^{\omega_2} \mathbf{v} = -\alpha_3^\top \mathbf{v} & 5) \alpha_2^\top \mathbf{L}_v^{\omega_2} \mathbf{v} = 0 & 6) \alpha_3^\top \mathbf{L}_v^{\omega_2} \mathbf{v} = \alpha_1^\top \mathbf{v} \\ 7) \alpha_1^\top \mathbf{L}_v^{\omega_3} \mathbf{v} = \alpha_2^\top \mathbf{v} & 8) \alpha_2^\top \mathbf{L}_v^{\omega_3} \mathbf{v} = -\alpha_1^\top \mathbf{v} & 9) \alpha_3^\top \mathbf{L}_v^{\omega_3} \mathbf{v} = 0 \end{array}$$

The constraints must be valid for any value of \mathbf{v} . They can be written under the form,

$$\begin{bmatrix} \mathbf{L}_v^{\omega_1 \top} & \mathbf{0} & \mathbf{0} \\ \mathbf{L}_v^{\omega_1 \top} & \mathbf{0} & -\mathbb{I} \\ \mathbf{L}_v^{\omega_1 \top} & \mathbb{I} & \mathbf{0} \\ \vdots & \vdots & \vdots \\ \mathbf{0} & \mathbf{0} & \mathbf{L}_v^{\omega_3 \top} \end{bmatrix} \begin{bmatrix} \alpha_1 \\ \alpha_2 \\ \alpha_3 \end{bmatrix} = \mathbf{0}, \quad (19)$$

where \mathbb{I} and $\mathbf{0}$ are respectively the identity and zero matrices of size $n \times n$ (e.g. $\mathbf{v} = \mathbf{v}_{(2,3)}^{(1,1)}$ is 60×60). The overview of the complete procedure to derive n -tuples in 3D space is shown in Table 1.

In the case of 2D distribution, the same framework allows obtaining n -tuples $\mathbf{x}_v = [\alpha_1^\top \mathbf{v} \ \alpha_2^\top \mathbf{v}]^\top$, called duoblet, that behave as a point in a plane with respect to rotations. As

examples, using $\mathbf{v}_{(2,3)}^{(1,1)}$ in 3D space, 3 triplets can be generated:

$$\begin{aligned} \mathbf{x}_{v1} &= \left[\begin{array}{l} m_{003}m_{101} + m_{012}m_{110} + m_{021}m_{101} + m_{030}m_{110} + m_{101}m_{201} \\ + m_{102}m_{200} + m_{110}m_{210} + m_{120}m_{200} + m_{200}m_{300} \\ m_{003}m_{011} + m_{011}m_{021} + m_{012}m_{020} + m_{020}m_{030} + m_{011}m_{201} \\ + m_{102}m_{110} + m_{020}m_{210} + m_{110}m_{120} + m_{110}m_{300} \\ m_{002}m_{003} + m_{002}m_{021} + m_{011}m_{012} + m_{011}m_{030} + m_{002}m_{201} \\ + m_{101}m_{102} + m_{011}m_{210} + m_{101}m_{120} + m_{101}m_{300} \end{array} \right] \\ \mathbf{x}_{v2} &= \left[\begin{array}{l} m_{002}m_{120} - 2m_{011}m_{111} + m_{020}m_{102} + m_{002}m_{300} - 2m_{101}m_{201} \\ + m_{102}m_{200} + m_{020}m_{300} - 2m_{110}m_{210} + m_{120}m_{200} \\ m_{002}m_{030} - 2m_{011}m_{021} + m_{012}m_{020} + m_{002}m_{210} + m_{012}m_{200} \\ - 2m_{101}m_{111} + m_{020}m_{210} + m_{030}m_{200} - 2m_{110}m_{120} \\ m_{002}m_{021} + m_{003}m_{020} - 2m_{011}m_{012} + m_{002}m_{201} + m_{003}m_{200} \\ - 2m_{101}m_{102} + m_{020}m_{201} + m_{021}m_{200} - 2m_{110}m_{111} \end{array} \right] \\ \mathbf{x}_{v3} &= \left[\begin{array}{l} m_{002}m_{102} + 2m_{011}m_{111} + m_{020}m_{120} + 2m_{101}m_{201} \\ + 2m_{110}m_{210} + m_{200}m_{300} \\ m_{002}m_{012} + 2m_{011}m_{021} + m_{020}m_{030} + 2m_{101}m_{111} \\ + 2m_{110}m_{120} + m_{200}m_{210} \\ m_{002}m_{003} + 2m_{011}m_{012} + m_{020}m_{021} + 2m_{101}m_{102} \\ + 2m_{110}m_{111} + m_{200}m_{201} \end{array} \right] \end{aligned} \quad (20)$$

In 2D space, using the vector of moments $\mathbf{v}_{(2,3)}^{(1,1)}$, 3 doublet can be generated as:

$$\begin{aligned} \mathbf{x}_{v1} &= \left[\begin{array}{l} m_{03}m_{11} - m_{02}m_{12} - m_{02}m_{30} + m_{11}m_{21} \\ m_{11}m_{12} - m_{03}m_{20} + m_{11}m_{30} - m_{20}m_{21} \end{array} \right] \\ \mathbf{x}_{v2} &= \left[\begin{array}{l} 2m_{03}m_{11} - 2m_{02}m_{12} - m_{02}m_{30} + m_{12}m_{20} \\ m_{02}m_{21} - m_{03}m_{20} + 2m_{11}m_{30} - 2m_{20}m_{21} \end{array} \right] \\ \mathbf{x}_{v3} &= \left[\begin{array}{l} 3m_{02}m_{12} - 2m_{03}m_{11} + 2m_{02}m_{30} + m_{20}m_{30} \\ m_{02}m_{03} + 2m_{03}m_{20} - 2m_{11}m_{30} + 3m_{20}m_{21} \end{array} \right] \end{aligned} \quad (21)$$

An extended example is given in the script¹ which provides a list of n-tuples computed from moments of different orders and in different original spaces 2-, 3- and 4-dimension.

4.3. Reflection transformation and symmetry

A reflection transformation is defined by a sign flip of one coordinate while leaving the rest unchanged. An example of reflection is the transformation defined by $\mathbf{x}' = \mathbf{F}\mathbf{x}$ subject to the coordinates change $x'_1 = x_1$, $x'_2 = -x_2$ and $x'_3 = x_3$. As for rotations, a reflection \mathbf{F} holds $\mathbf{F}^T\mathbf{F} = \mathbf{I}$, but with $\det(\mathbf{F}) = -1$. The effect of such transformation on a moment is given by,

$$m'_{p_1p_2p_3} = (-1)^{p_2}m_{p_1p_2p_3}. \quad (22)$$

If the sign changing was on x_1 , the effect on moment would be $m'_{p_1p_2p_3} = (-1)^{p_1}m_{p_1p_2p_3}$. If a n -tuple undergoes the same reflection as the object points, the vectors of coefficients will have to hold $\alpha_1\mathbf{v}' = \alpha_1\mathbf{v}$, $\alpha_2\mathbf{v}' = -\alpha_2\mathbf{v}$ and $\alpha_3\mathbf{v}' = \alpha_3\mathbf{v}$, where \mathbf{v}' is obtained from \mathbf{v} using eq. (22). Surprisingly, for the different set of n -tuples obtained by solving eq. (19), they already hold the reflection conditions.

¹https://drive.google.com/file/d/1UF-5FANGIxAnVq1jLQm2h_f8d3BxpRo7/view?usp=sharing

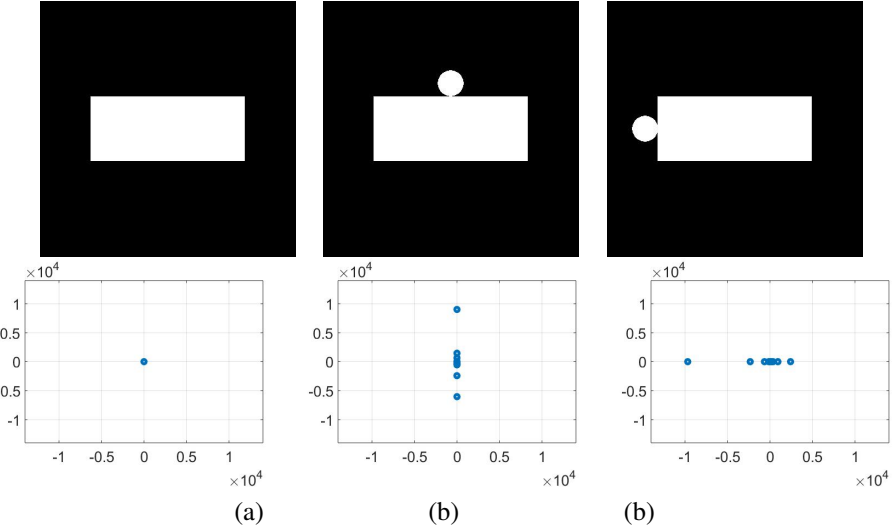


Figure 1: Case study of symmetry: (a) object center, (b) x-axis (c) y-axis

Now, let us assume that the object is symmetrical with respect to the plane x_1x_3 . For such object, the considered reflection example will leave its shape unchanged. Since the moment n -tuples undergo the same reflection, they must belong to the plane x_1x_3 . Otherwise, one can make difference between the distribution configurations before and after reflection. In fact, this is valid for any plane of symmetry, since the n -tuples undergo the same rotation as that applied to an object. The same reasoning can be used for other kinds of symmetries.

Note that we can obtain the symmetry plane via Singular Value Decomposition (SVD) of the n -tuple. Concretely, the singular vector that describes the symmetry plane is the one associated with minimal singular value. The type of symmetry is determined by the relationship among the different singular values. In addition, two non-aligned triplets are enough to estimate orthogonal transformation (rotation or reflection) since they can build an orthogonal base of the object. But, with more than two triplets the rotations can be found using Procrustes methods Schönenmann (1966).

5. Experiments in 2D space

We examine how the n -tuples in 2D behave under the effect of adding non-symmetry transformation on a controlled example (Fig. 1). For each image, doublets are computed from the moment vectors $\mathbf{v}_{(2,3)}^{(1,1)}, \mathbf{v}_{(2,5)}^{(1,1)}, \mathbf{v}_{(4,3)}^{(1,1)}, \mathbf{v}_{(4,5)}^{(1,1)}, \mathbf{v}_{(6,3)}^{(1,1)}, \mathbf{v}_{(6,5)}^{(1,1)}, \mathbf{v}_{(6,7)}^{(1,1)}, \mathbf{v}_{(6,9)}^{(1,1)}, \mathbf{v}_{(8,7)}^{(1,1)}$ and $\mathbf{v}_{(8,9)}^{(1,1)}$. For the rectangle given in Fig. 1(a) top, the corresponding n -tuples coincide with the origin since the object is symmetrical with respect to its center (Fig. 1(a) bottom). For the two objects shown in Fig. 1(b) and Fig. 1(c), they exhibit symmetries with respect to two different axis. They were obtained by adding a disc to the rectangle in specific positions. Their doublets are shown in the bottom row of Fig. 1(b) and Fig. 1(c). The plots show that their n -tuples form lines in the directions of their respective symmetry axis.

In another experiment, shown in Fig. 2(a), the considered object does not exhibit any symmetry. This time, doublets were computed separately from the vector moments $\mathbf{v}_{(2,3)}^{(1,1)}, \mathbf{v}_{(4,5)}^{(1,1)}$, and

$\mathbf{v}_{(6,3)}^{(1,1)}$. The obtained results are shown in Fig. 2(b) for $\mathbf{v}_{(2,3)}^{(1,1)}$, Fig. 2(c) for $\mathbf{v}_{(4,5)}^{(1,1)}$ and Fig. 2(d) for $\mathbf{v}_{(6,3)}^{(1,1)}$. The figures show that asymmetries are more noticeable for doublets computed from moment of higher order. Indeed, the obtained ratios, using SVD decomposition, between the higher and smaller singular values of the doublets were 8.73, 2.71 and 5.59 for $\mathbf{v}_{(2,3)}^{(1,1)}$, $\mathbf{v}_{(4,5)}^{(1,1)}$, and $\mathbf{v}_{(6,3)}^{(1,1)}$ respectively. In general, the smaller a ratio is, farthest the n -tuples is for forming a line. A last experiment, illustrated in Fig. 3, explores approximate mirror symmetry. For the considered objects, the images are first converted to gray-scale then to binary. The doublets are computed using centered moments of the binary image. Finally, the lines of symmetry are estimated using the direction corresponding to the smaller singular value of the doublets.

6. Experiments in 3D space

The goal of this part is to validate the symmetry detection as well as orthogonal transformations using triplets. The used objects are part of the datasets McGill University ² and ShapeNet Chang et al. (2015). In both cases, objects are not completely symmetrical. As for images case, n -tuples are computed from the central moments of different orders.

6.1. Symmetry with respect to a plane

We deal with symmetry detection and rotation estimation in this experiment. The chosen object to conduct this experiment is a random mug (Fig. 4) from ShapeNet. Fig. 4(a) shows the object model in their original pose $\mathbb{I} \in \mathbb{R}^{3 \times 3}$ and Fig. 4(b) shows it after being applied the rotation $\mathbf{R} \in \text{SO}(3)$ defined as follows,

$$\mathbf{R} = \begin{bmatrix} -0.3085 & 0.2118 & 0.9273 \\ 0.8599 & -0.3546 & 0.3671 \\ 0.4066 & 0.9106 & -0.0727 \end{bmatrix}. \quad (23)$$

For the two considered mug poses, the obtained singular vectors are respectively \mathbf{V} and \mathbf{V}_R (eq. 24), holding two equal singular values $\mathbf{S} = \mathbf{S}_R$ (eq. 25). This shows the equivalent relationship between the geometric transformation of the model and the n -tuples transformation for the single plane symmetry case. Since the shape of the distribution is hold during orthogonal transformation $\text{SO}(3)$, that is, the singular values keep constants. But their singular values are transformed equally to the geometric transformation of the 3D object model (Fig. 4(c)).

²<http://www.cim.mcgill.ca/shape/benchMark/>

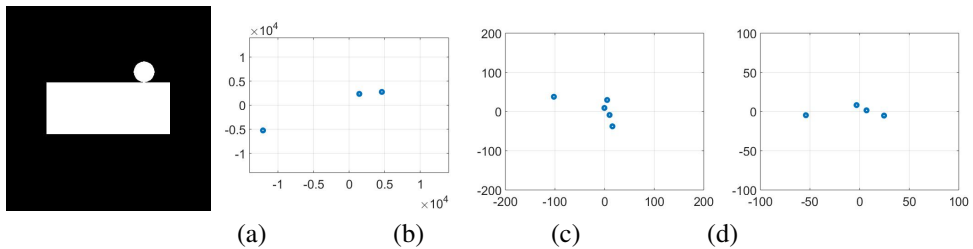


Figure 2: Case study of a non-symmetrical object: (a) the object, (b) n -tuples from $\mathbf{v}_{(2,3)}^{(1,1)}$, (c) n -tuples from $\mathbf{v}_{(4,5)}^{(1,1)}$, (d) n -tuples from $\mathbf{v}_{(6,3)}^{(1,1)}$

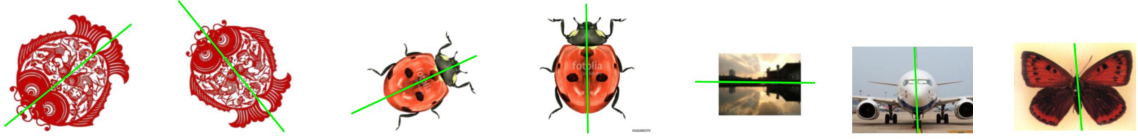


Figure 3: Example of mirror symmetry

$$\mathbf{V} = \begin{bmatrix} -0.001 & 0.027 & 0.999 \\ -0.343 & 0.938 & -0.026 \\ 0.939 & 0.342 & -0.007 \end{bmatrix}; \mathbf{V}_R = \mathbf{R} \mathbf{V} \quad (24)$$

In addition, it can be estimated the type of symmetry from the shape of the moment's n -tuples, i.e. singular values. Let σ_1 , σ_2 , and σ_3 be the singular values, such as $\sigma_1 > \sigma_2 > \sigma_3$, and v_1 , v_2 , v_3 their corresponding singular vectors. The relation between the two smallest singular values and the biggest one determine the type of symmetry. Such as, if the $\frac{\sigma_1}{\sigma_3}$ is orders of magnitude bigger than $\frac{\sigma_1}{\sigma_2}$, the symmetry is planar. This is due to the existence of a dominant symmetry plane. In the specific case, Fig. 4(a), we have that $\frac{\sigma_1}{\sigma_3} = 1121.22$ and $\frac{\sigma_1}{\sigma_2} = 17.40$. Meaning that, the n -tuples, triplets, form a plane of symmetry defined by v_3 , i.e. the third column of the matrix \mathbf{V} , eq. (24).

$$\mathbf{S}_R = \begin{bmatrix} 3.2705 & 0.1879 & 0.0029 \end{bmatrix} \cdot 10^5 = \mathbf{S} \quad (25)$$

Finally, the estimation of the orthogonal rotational transformation between both distributions, objects, poses is obtained as a generalized solution of the orthogonal Procrustes problem between the two set of moments n -tuples computed in Table 1. The real and estimated values of the rotation matrix are given by eq. (26), recovering the original transformation, eq. (23):

$$\widehat{\mathbf{R}} = \begin{bmatrix} -0.3085 & 0.2118 & 0.9273 \\ 0.8599 & -0.3546 & 0.3671 \\ 0.4066 & 0.9106 & -0.0727 \end{bmatrix} = \mathbf{R} \quad (26)$$

The obtained result shows that the estimation is quite accurate. Note also that $\mathbf{V}_R = \mathbf{R} \mathbf{V}$. Which means that the plane of symmetry undergoes the same rotation to the object.

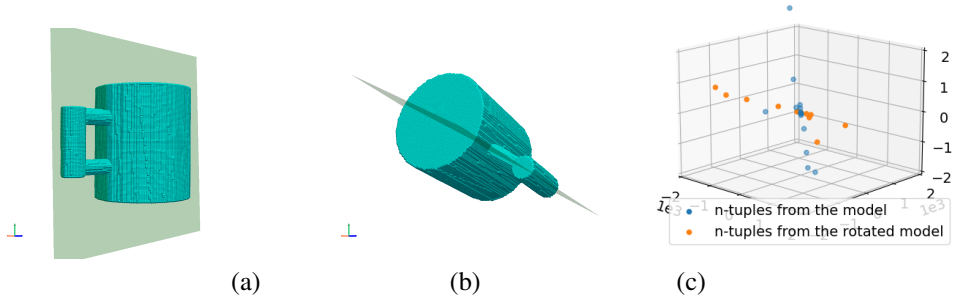


Figure 4: Mug, a symmetrical object case of study: (a) Plane of symmetry of the object with initial conditions, $\mathbf{R} = \mathbb{I}$. (b) Plane of symmetry recovered after being applied to a random \mathbf{R} rigid transformation. (c) Representation of moment's n -tuples in Cartesian space.

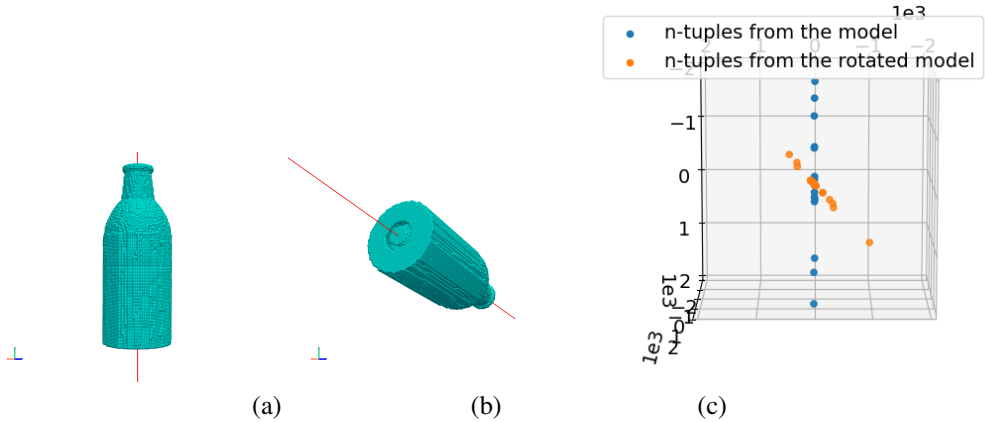


Figure 5: Axial symmetry: (a) bottle model, (b) the rotated bottle, (c) the n -tuples computed from moments

6.2. Symmetry with respect to a radial axis

In order to show how moments n -tuples deal with radial symmetry, we present the following case study. Concretely, this experiment shows the model of a generic bottle with a radial symmetry axis (Fig. 5(a)). As for the previous case, both considered object poses are: aligned to the global frame, y-axis up-direction and z-axis forward direction; and obtained by applying a random transformation.

The ratios of singular values are $\frac{\sigma_1}{\sigma_3} = 1926.33$ and $\frac{\sigma_1}{\sigma_2} = 149.99$. Differently from the mug case (Fig. 4), here the distance between both ratios is one order of magnitude smaller. The intersection of the planes defined the two singular vectors v_2, v_3 corresponding to the smaller singular values defines the symmetry axis as shown in Fig. 5(a) and Fig. 5(b). Finally, the n -tuples positions are shown in Fig. 5(c). They show that they almost belong to the symmetry axis for the two bottle poses.

$$\mathbf{S} = \begin{bmatrix} 9.3904 & 0.0626 & 0.0048 \end{bmatrix} \cdot 10^4 = \mathbf{S}_R \quad (27)$$

6.3. Boosting b -plane symmetry by axial symmetry

This section addresses objects exhibiting symmetry concerning multiple planes and their rotation around a central axis. Specifically, these objects possess b symmetry planes. An illustrative

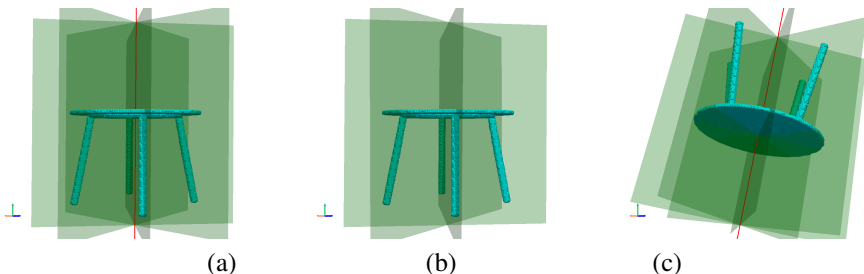


Figure 6: n -plane symmetry case: (a) table model, (b) the rotated table with added noise, (c) the n -tuples computed from moments

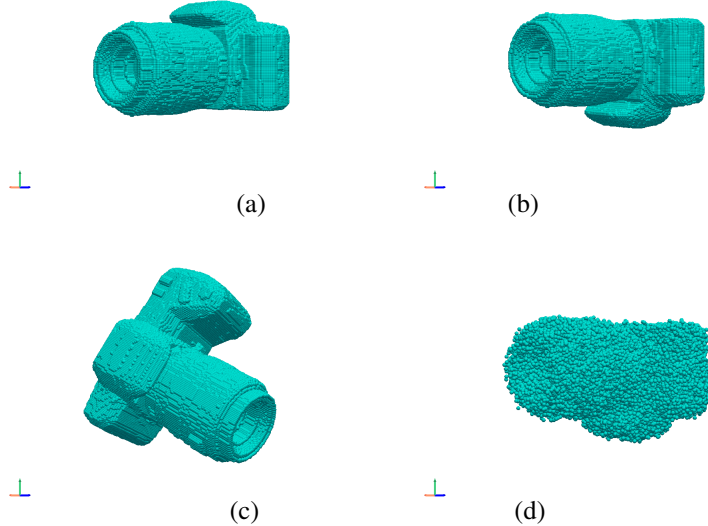


Figure 7: Reflection estimation using camera model: (a) model, (b) after reflection, (c) after reflection then rotation, (d) , (e) noisy model

example is provided by the model of a four-legged table depicted in Fig. 6. This table exhibits four distinct symmetry planes: two located between the legs and two intersecting them.

This issue can be addressed through iterative approximation methods, as demonstrated in the works of Funk et al. (2017); Ecins et al. (2017); Nagar and Raman (2020b); Cicconet et al. (2017). However, the accuracy and ability of iterative solutions to detect all planes depend on their initialization. Therefore, by initializing the problem close to the optimal solution, we stabilize the convergence and enhance performance.

To illustrate how the n -tuples description can be integrated with iterative methods, we employed the method proposed in Ecins et al. (2017) to solve the problem of b symmetrical planes, augmented by our proposed method presented in sections 3 and 4. In this experiment, the estimated axial symmetry from moment n -tuples serves as a suitable candidate for initializing the search for b -planes of symmetry.

The residual function, as proposed in Ecins et al. (2017), and its gradient are defined using a single random variable θ , which rotates the symmetry plane \vec{S} as follows,

$$e = \left(\mathbf{R}^{[\theta \vec{v}; \vec{S}]} \mathbf{F} \left(\mathbf{R}^{[\theta \vec{v}; \vec{S}]} \right)^{-1} \mathbf{x}_u - \mathbf{x}_l \right) \vec{n}_l ,$$

where \mathbf{x}_u and \mathbf{x}_l are respectively upper and lower 3D points with respect to the symmetry plane defined by \vec{S} . And \vec{n}_l is the orientation of the lower point \mathbf{x}_l . Remark, that $\mathbf{R}^{[\cdot]}$ function represent the argument of an orthogonal transformation $\text{SO}(3)$ and \mathbf{F} is a diagonal matrix defined by the vector $[-1, 1, -1]$. This formulation decrements the number of iteration to converge to a correct solution, beside with the improvement of computational cost per iteration. In the case of Fig. 6, the n -tuples iterative method recover all 4 planes of symmetry after 3 iteration. While the baseline iterative method succeeded to get 3 planes of symmetry after 10 iterations (Fig. 6 (b)).

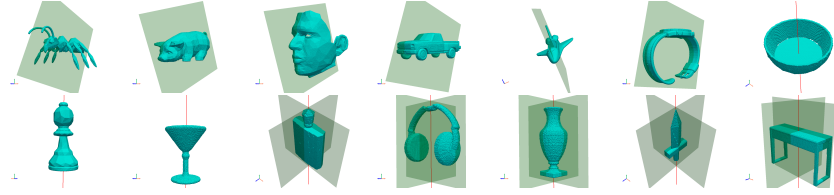


Figure 8: Examples of symmetry with respect to a plane and to an axis

6.4. Reflection estimation

In this last experiment, we validate orthogonal transformation estimation using a non-symmetrical object, particularly the used model is a reflex camera (Fig. 7). We consider three different poses in order to conduct the following experiment. The reference one, is aligned to the world frame, the second one is generated by applying a reflection transformation \mathbf{F} defined in eq. (28), and the third one is obtained by applying a random rotation transformation \mathbf{R} after applying \mathbf{F} to original pose eq. (29) (Fig. 7 (c)). As it can be observed, moments n -tuples recover the $\text{SO}(3)$ and reflection transformations in absence of noise. These properties it is conserved no matters if the object is symmetrical or not.

$$\mathbf{F} = \begin{bmatrix} 1 & 0 & 0 \\ 0 & -1 & 0 \\ 0 & 0 & 1 \end{bmatrix} = \widehat{\mathbf{F}} \quad (28)$$

$$\mathbf{R}_F = \begin{bmatrix} -0.3085 & 0.2118 & 0.9273 \\ -0.8599 & 0.3546 & -0.3671 \\ 0.4066 & 0.9106 & -0.0727 \end{bmatrix} = \widehat{\mathbf{R}}_F \quad (29)$$

Finally, for the same experiments, we add Gaussian noise $\mathcal{N}(0 | 5 \cdot 10^3)$ (Fig. 7 (d)) in order to demonstrate the performance of our method under noise conditions. As it is shown in eq. (30) and eq. (31) in both cases recovered transformations are close to the optimal solution. Concretely, both have a similar deviation of $1 \cdot 10^{-2}$ using mean squared error of the differences.

$$\mathbf{F} = \begin{bmatrix} 1 & 0 & 0 \\ 0 & -1 & 0 \\ 0 & 0 & 1 \end{bmatrix} \approx \widehat{\mathbf{F}} \quad (30)$$

$$\mathbf{R}_F = \begin{bmatrix} 0.466 & 0.546 & 0.695 \\ 0.846 & -0.048 & -0.530 \\ 0.256 & -0.835 & 0.485 \end{bmatrix} \approx \widehat{\mathbf{R}}_F \quad (31)$$

As final validation results, Fig. 8 shows the application of the method using moments n -tuples under different conditions: reflection; axial; and b -plane symmetrical. It can be seen that the obtained results are consistent with the discussed above. Hence, the effectiveness of the proposed scheme. The source code and 28 object example can be downloaded from the following URL³.

³https://drive.google.com/file/d/1ija_bMnA3IOSXmdGsRqzA1_EbZFc5tcw/view?usp=sharing

7. Conclusion and future works

This paper has proposed unique measures called moments n -tuples to detect symmetries and to estimate orthogonal transformations, including reflections in n -dimensional space. Here, we focus the analysis concretely in 2 and 3-dimensional cases, but it is extensible to n dimensional problems. We show that those two properties, symmetry and orthogonal transformation, are linked in our proposed moments n -tuples space. Besides, note that symmetry affects rotation observability since it causes ambiguity on its estimation. This can be seen through the distribution of the n -tuples in the space. The validation results show that the proposed method is able to detect symmetry even for object that are not completely symmetrical. They also show a low computation cost. Future works will be devoted to extend the obtained results to affine transformation estimation instead of only orthogonal ones. In fact, if a continuous distribution in \mathbb{R}^2 undergoes an affine transformation, we can show for instance that the doublet, defined as follows,

$$\mathbf{x}_a = \frac{1}{m_{00}^4} \begin{bmatrix} m_{02}m_{30} - 2m_{11}m_{21} + m_{12}m_{20} \\ m_{02}m_{21} + m_{03}m_{20} - 2m_{11}m_{12} \end{bmatrix}$$

will undergo the same transformation as the source distribution. We will be concerned with a general scheme for determining affine n -tuples in n -dimensional space.

References

- Aguilar, W., Alvarado-Gonzalez, M., Garduño, E., Velarde, C., Bribiesca, E., 2020. Detection of rotational symmetry in curves represented by the slope chain code. *Pattern Recognition* 107, 107421.
- Alt, H., Mehlhorn, K., Wagener, H., Welzl, E., 1988. Congruence, similarity, and symmetries of geometric objects. *Discrete & Computational Geometry* 3, 237–256.
- Atallah, M., 1985. On symmetry detection. *IEEE Transactions on Computers* 34, 663–666.
- Chang, A.X., Funkhouser, T., Guibas, L., Hanrahan, P., Huang, Q., Li, Z., Savarese, S., Savva, M., Song, S., Su, H., et al., 2015. Shapenet: An information-rich 3d model repository. *arXiv preprint arXiv:1512.03012* “. *arXiv:quant-ph/1512.03012*.
- Chen, Y., Sareh, P., Feng, J., Sun, Q., 2017. A computational method for automated detection of engineering structures with cyclic symmetries. *Computers & Structures* 191, 153–164.
- Chen, Z., Sun, S.K., 2010. A Zernike moment phase-based descriptor for local image representation and matching. *IEEE Transactions on Image Processing* 19, 205–219.
- Cicconet, M., Hildebrand, D.G.C., Elliott, H., 2017. Finding mirror symmetry via registration and optimal symmetric pairwise assignment of curves, in: 2017 IEEE International Conference on Computer Vision Workshops (ICCVW), IEEE, Venice, Italy. pp. 1749–1758.
- Cyganski, D., Orr, J.A., 1985. Applications of tensor theory to object recognition and orientation determination. *IEEE Transactions on Pattern Analysis and Machine Intelligence PAMI-7*, 662–673.
- Derrode, S., Ghorbel, F., 2004. Shape analysis and symmetry detection in gray-level objects using the analytical fourier–mellin representation. *Signal processing* 84, 25–39.

- Ecins, A., Fermuller, C., Aloimonos, Y., 2017. Detecting reflectional symmetries in 3d data through symmetrical fitting, in: Proceedings of the IEEE International Conference on Computer Vision Workshops, IEEE, Venice, Italy. pp. 1779–1783.
- Fortenberry, C., Bowman, E.A., Proffitt, W., Dorr, B., Combs, S., Harp, J., Mizoue, L., Meiler, J., 2011. Exploring symmetry as an avenue to the computational design of large protein domains. *Journal of the American Chemical Society* 133, 18026–18029.
- Funk, C., Lee, S., Oswald, M.R., Tsogkas, S., Shen, W., Cohen, A., Dickinson, S., Liu, Y., 2017. 2017 iccv challenge: Detecting symmetry in the wild, in: 2017 IEEE International Conference on Computer Vision Workshops (ICCVW), IEEE, Venice, Italy. pp. 1692–1701.
- Gao, L., Zhang, L.X., Meng, H.Y., Ren, Y.H., Lai, Y.K., Kobbelt, L., 2020. Prs-net: Planar reflective symmetry detection net for 3d models. *IEEE Transactions on Visualization and Computer Graphics* 27, 3007–3018.
- Gent, I.P., Petrie, K.E., Puget, J.F., 2006. Symmetry in constraint programming. *Foundations of Artificial Intelligence* 2, 329–376.
- Huang, J.B., Kang, S.B., Ahuja, N., Kopf, J., 2014. Image completion using planar structure guidance. *ACM Transactions on graphics (TOG)* 33, 1–10.
- Ji, P., Liu, X., 2019. A fast and efficient 3d reflection symmetry detector based on neural networks. *Multimedia Tools and Applications* 78, 35471–35492.
- Krippendorf, S., Syvaeri, M., 2020. Detecting symmetries with neural networks. *Machine Learning: Science and Technology* 2, 015010.
- Lederman, S.J., Wing, A.M., 2003. Perceptual judgement, grasp point selection and object symmetry. *Experimental Brain Research* 152, 156–165.
- Li, W.H., Zhang, A.M., Kleeman, L., 2005. Fast global reflectional symmetry detection for robotic grasping and visual tracking, in: Proceedings of Australasian Conference on Robotics and Automation, December. pp. 147–151.
- Liu, Y., Hel-Or, H., Kaplan, C.S., 2010. Computational symmetry in computer vision and computer graphics. Now publishers Inc.
- Liu, Z.J., Li, Q., Xia, Z.W., Wang, Q., 2012. Target recognition of ladar range images using even-order Zernike moments. *Applied optics* 51, 7529–7536.
- Margot, F., 2009. Symmetry in integer linear programming. *50 Years of Integer Programming 1958-2008: From the Early Years to the State-of-the-Art* , 647–686.
- Markandey, V., deFigueiredo, R., 1992. Robot sensing techniques based on high-dimensional moment invariants and tensors. *IEEE transactions on robotics and automation* 8, 186–195.
- Martinet, A., Soler, C., Holzschuch, N., Sillion, F.X., 2006. Accurate detection of symmetries in 3D shapes. *ACM Transactions on Graphics (TOG)* 25, 439–464.
- Mitra, N.J., Wand, M., Zhang, H., Cohen-Or, D., Kim, V., Huang, Q.X., 2014. Structure-aware shape processing, in: ACM SIGGRAPH 2014 Courses, pp. 1–21.

- Mukundan, R., Ramakrishnan, K., 1998. Moment functions in image analysis—theory and applications. World Scientific, London.
- Nagar, R., Raman, S., 2020a. 3dsymm: robust and accurate 3d reflection symmetry detection. *Pattern Recognition* 107, 107483.
- Nagar, R., Raman, S., 2020b. 3dsymm: Robust and accurate 3d reflection symmetry detection. *Pattern Recognition* 107, 1–11.
- Schönemann, P.H., 1966. A generalized solution of the orthogonal procrustes problem. *Psychometrika* 31, 1–10.
- Shen, D., Ip, H.H.S., Cheung, K.K., Teoh, E.K., 1999. Symmetry detection by generalized complex (gc) moments: a close-form solution. *IEEE Transactions on Pattern Analysis and Machine Intelligence* 21, 466–476.
- Shi, Y., Huang, J., Zhang, H., Xu, X., Rusinkiewicz, S., Xu, K., 2020. Symmetrynet: Learning to predict reflectional and rotational symmetries of 3d shapes from single-view rgb-d images. *ACM Transactions on Graphics (TOG)* 39, 1–14.
- Sluzek, A., 1995. Identification and inspection of 2-D objects using new moment-based shape descriptors. *Pattern Recognition Letters* 16, 687–697.
- Song, C., Song, J., Huang, Q., 2020. Hybridpose: 6d object pose estimation under hybrid representations, in: Proceedings of the IEEE/CVF conference on computer vision and pattern recognition, pp. 431–440.
- Speciale, P., Oswald, M.R., Cohen, A., Pollefeys, M., 2016. A symmetry prior for convex variational 3d reconstruction, in: European Conference on Computer Vision, Springer, Amsterdam, the Netherlands. pp. 313–328.
- Tahri, O., 2004. Utilisation des moments en asservissement visuel et en calcul de pose. Ph.D. thesis. Rennes 1.
- Tahri, O., Chaumette, F., 2003. Determination of moment invariants and their application to visual servoing. Technical Report 1539. IRISA.
- Tahri, O., Chaumette, F., 2005. Point-based and region-based image moments for visual servoing of planar objects. *IEEE Transactions on Robotics* 21, 1116–1127.
- Tahri, O., Mezouar, Y., Chaumette, F., Corke, P., 2010. Decoupled image-based visual servoing for cameras obeying the unified projection model. *IEEE Transactions on Robotics* 26, 684–697.
- Tayangkanon, T., Sompagdee, P., Li, X., 2018. 3d model compression over ascii encoded using rotational and reflective symmetry, in: 2018 10th International Conference on Knowledge and Smart Technology (KST), IEEE, Chiang Mai, Thailand. pp. 53–58.
- Wang, D., He, C., Li, X., Peng, J., 2015a. Progressive point set surface compression based on planar reflective symmetry analysis. *Computer-Aided Design* 58, 34–42.

- Wang, Z., Tang, Z., Zhang, X., 2015b. Reflection symmetry detection using locally affine invariant edge correspondence. *IEEE Transactions on Image Processing* 24, 1297–1301.
- Widynski, N., Moevus, A., Mignotte, M., 2014. Local symmetry detection in natural images using a particle filtering approach. *IEEE Transactions on Image Processing* 23, 5309–5322.
- Wolter, J.D., Woo, T.C., Volz, R.A., 1985. Optimal algorithms for symmetry detection in two and three dimensions. *The Visual Computer* 1, 37–48.
- Wong, W.H., Siu, W.C., Lam, K.M., 1995. Generation of moment invariants and their uses for character recognition. *Pattern Recognition Letters* 16, 115–123.
- Zhang, P., Fan, W., Chen, Y., Feng, J., Sareh, P., 2022. Structural symmetry recognition in planar structures using convolutional neural networks. *Engineering Structures* 260, 114227.
- Zhou, Y., Liu, S., Ma, Y., 2021. Nerd: Neural 3d reflection symmetry detector, in: *Proceedings of the IEEE/CVF Conference on Computer Vision and Pattern Recognition*, pp. 15940–15949.
- Zingoni, A., 2012. Symmetry recognition in group-theoretic computational schemes for complex structural systems. *Computers & structures* 94, 34–44.